

# Observation of the Aerosol Plume From the 2022 Hunga Tonga – Hunga Ha’apai Eruption With SAGE III/ISS

Clair Duchamp<sup>1</sup>, Felix Wrana<sup>2</sup>, Bernard Legras<sup>1</sup>, Pasquale Sellitto<sup>3,4</sup>, Redha Belhadji<sup>3</sup>, Christian von Savigny<sup>2</sup>

<sup>1</sup>Laboratoire de Météorologie Dynamique (LMD-IPSL), CNRS, Sorbonne Université, ENS-PSL, École Polytechnique, Paris, France

<sup>2</sup>Institute of Physics, University of Greifswald, Greifswald, Germany

<sup>3</sup>Université Paris Est Créteil and Université de Paris-Cité, CNRS, Laboratoire Interuniversitaire des Systèmes Atmosphériques (LISA-IPSL), Créteil, France

<sup>4</sup>Istituto Nazionale di Geofisica e Vulcanologia (INGV), Osservatorio Etneo (OE), Catania, Italy

## Key Points:

- The extinction of the stratospheric plume of the 2022 Tonga eruption is well modeled by a unimodal distribution of sulfate particles
- The effective radius of the aerosols is large with values close to 0.4  $\mu\text{m}$ , and a mode width of 1.25, from March 2022 to June 2023
- We estimate a total  $\text{H}_2\text{SO}_4$  mass in stratospheric sulfate aerosols of about 0.66 Tg corresponding to 0.44 Tg of  $\text{SO}_2$  initially injected

Received: 20 JUNE 2023

Accepted: 23 AUGUST 2023

DOI: 10.1029/2023GL105076

---

Corresponding author: Clair Duchamp, [clair.duchamp@lmd.ipsl.fr](mailto:clair.duchamp@lmd.ipsl.fr)

## Abstract

The Tonga eruption of 15 January 2022 has released a long-lived stratospheric plume of sulfate aerosols. More than 17 months after, we focus on the high quality data series of SAGE III (Stratospheric Aerosol and Gas Experiment) on board the International Space Station (ISS) to determine the mean radius and size distribution of the aerosols and their total mass. The persisting volcanic aerosols – with a mode width of 1.25 and an effective radius of 0.4  $\mu\text{m}$  – differ from the significantly smaller background aerosols and from those measured during recent stratospheric eruptions. The sulfuric acid mass between 50°S and 30°N is estimated to be very stable in spite of considerable redistribution in latitude at a value of  $0.66 \pm 0.1$  Tg, corresponding to an initial sulfur dioxide emission of 0.44 Tg. Such properties are expected to facilitate the persistence of a climate warming due to the volcanic water vapour.

## Plain Language Summary

We study the stratospheric aerosol plume produced by the Hunga Tonga–Hunga Ha’apai eruption on 15 January 2022 based on the high quality solar occultation measurements of the instrument SAGE III (Stratospheric Aerosol and Gas Experiment) on-board the International Space Station. These data reveal that the aerosol sizes are about twice as large as after other documented volcanic eruptions and that the total mass of  $\text{H}_2\text{SO}_4$  in the liquid droplets of sulfate in the stratosphere has been very stable from March 2022, when it started to be well homogenized in longitude, to November 2022, when it started to decay. The total mass of 0.66 Tg of  $\text{H}_2\text{SO}_4$  is in good agreement with the early estimates of a stratospheric emission of 0.4–0.5 Tg of  $\text{SO}_2$ . The implication is that the aerosol radiative impact will not mask the persisting warming effect of the water vapour injected in the stratosphere by the eruption.

## 1 Introduction

The phreato-magmatic eruption of the Hunga Tonga–Hunga Ha’apai (HTHH) started on 20 December 2021 and went through an explosive phase on 15 January 2022 which was comparable in Volcanic Explosivity Index with Pinatubo (Poli & Shapiro, 2022). The atmospheric plume was exceptional by reaching the mesosphere with a maximum height of 58 km and by injecting a considerable amount of water that saturated the stratosphere at least up to 35 km leaving a +10% increase of the stratospheric water vapour (Carr et al., 2022; Millán et al., 2022; Khaykin et al., 2022). The initial injection of water might have been much larger as the estimated amount of solid ejecta is close to 7 km<sup>3</sup> (O’Callaghan, 2022) but the water in excess above saturation condensed rapidly and precipitated entraining the ash that mostly disappeared from the stratosphere (Legras et al., 2022). As a matter of fact, besides a thin cloud detected at 35 km during a few days (Khaykin et al., 2022; Baron et al., 2023), no depolarizing aerosols have been detected in the stratosphere above 18 km in the aftermath of the eruption (Legras et al., 2022), indicating that ash did not play an important role. In contrast to water, the early estimates of the  $\text{SO}_2$  injection at 0.4–0.5 Tg (Millán et al., 2022; Carn et al., 2022) were modest compared to the  $18 \pm 4$  Tg of Pinatubo (Guo et al., 2004) and even to the 1.5 Tg of Raikoke (de Leeuw et al., 2021). However, the moist environment induced a fast conversion to sulfate aerosols (SA) (Zhu et al., 2022) that were detected as non depolarizing, presumably spherical, particles and the conversion was basically complete by the end of January (Legras et al., 2022). It was suggested that the initial estimate could have missed a large amount of already converted  $\text{SO}_2$  and estimates of up to 1.5 Tg have been speculated on (Sellitto et al., 2022; Legras et al., 2022). Several estimates of the average size of the aerosols and of their evolution ranging from 0.2 to 1  $\mu\text{m}$  have been provided from satellite retrievals and in situ measurements (Kloss et al., 2022; Schoeberl et al., 2022; Taha et al., 2022; Legras et al., 2022; Khaykin et al., 2022; Baron et al., 2023; Boichu et al., 2023). Such

dispersion has considerable impact on the persistence of aerosols in the stratosphere and their radiative impact (Zhu et al., 2022; Sellitto et al., 2022; Zhang et al., 2022). More than 17 months after the eruption, the goal of this work is to provide a well documented survey of the size and distribution of the aerosols, using minimal assumptions by taking advantage of the high quality measurements of SAGE III/ISS.

## 2 Data and Methods

### 2.1 SAGE III/ISS

The instrument Stratospheric Aerosol and Gas Experiment III (SAGE III), onboard the International Space Station (ISS), has been providing measurements of solar and lunar occultation since June 2017 (Cisewski et al., 2014). The instrument provides aerosol extinctions at nine wavelengths from 384 to 1,543 nm, the latter near-infrared channel being an addition with respect to SAGE II which significantly extends the spectral range. The data are provided in 0.5 km steps between 0 and 45 km altitude. The instrument observes about 15 sunrises and 15 sunsets per day with a latitudinal range which varies depending on the period of year (cf. Table S1). In particular, there are no profiles at higher latitudes than 50°S between May and July. The aerosol extinctions are retrieved as residuals of a spectral multilinear fit for O<sub>3</sub> and N<sub>2</sub>O but do not require any size distribution assumptions unlike instruments with limb-scatter geometry like OMPS-LP (Loughman et al., 2018).

For this study, we use the version 5.3 of the SAGE III/ISS level 2 solar aerosol product. The profiles are monthly averaged in four latitude bands of width  $\Delta\phi = 20^\circ$ , using data from November 2021 to June 2023. Due to its sparse geographical sampling, SAGE III began to see the HTHH SA plume only in March 2022 limiting our approach to the months beyond March 2022. During January and February 2022, SAGE III seldom sampled the plume and data are used for comparison between the plume and background conditions.

### 2.2 Retrieval of Aerosol Size Parameters at 3 Wavelengths

We use a method implemented by Wrana et al. (2021) to retrieve the SA size distribution which is based on the two color ratios 449/755 nm and 1,543/755 nm for the aerosol extinction coefficients. These ratios are modeled for spherical liquid SA through Mie calculations using miepython, a python code where the Mie theory is implemented following the procedure described by Wiscombe (1979). We use fixed refractive indices from the GEISA spectroscopic database (Armante et al., 2016), for a temperature of 215 K and a H<sub>2</sub>SO<sub>4</sub> weight proportion  $w_s$  of 70 % considering that the rest of the liquid droplet is water (Biermann et al., 2000), that is  $\{n_{449}, n_{755}, n_{1543}\} = \{1.439, 1.438, 1.42\}$ . This weight proportion has been obtained according to Tabazadeh et al. (1997) using ambient temperature and moisture of the plume (see Section S2). As the SA have a very low absorption in the shortwave spectral range (Palmer & Williams, 1975), we fix the imaginary part of the refractive index to  $10^{-6}$ . Due to the presumed absence of ash, we assume that the particle size distribution (PSD) follows a monomodal lognormal distribution law.

$$\mathcal{N} = \frac{N_0}{\sqrt{2\pi r \ln \sigma}} \exp\left(-\frac{\ln^2(r/r_m)}{2 \ln^2 \sigma}\right) \quad (1)$$

where  $\sigma$  is the mode width,  $r_m$  is the median radius, and  $N_0$  is the number density. The aerosol extinction  $k_{ext}$  at wavelength  $\lambda$  is then obtained by an integration over the size distribution.

$$k_{ext}(\lambda) = \int_0^{+\infty} Q_{ext}(r, n, \lambda) \cdot \pi r^2 \cdot \mathcal{N}(r, r_m, \sigma, N_0) dr \quad (2)$$

where  $Q_{ext}$  is the extinction efficiency factor from Mie calculations and  $n$  is the refractive index.

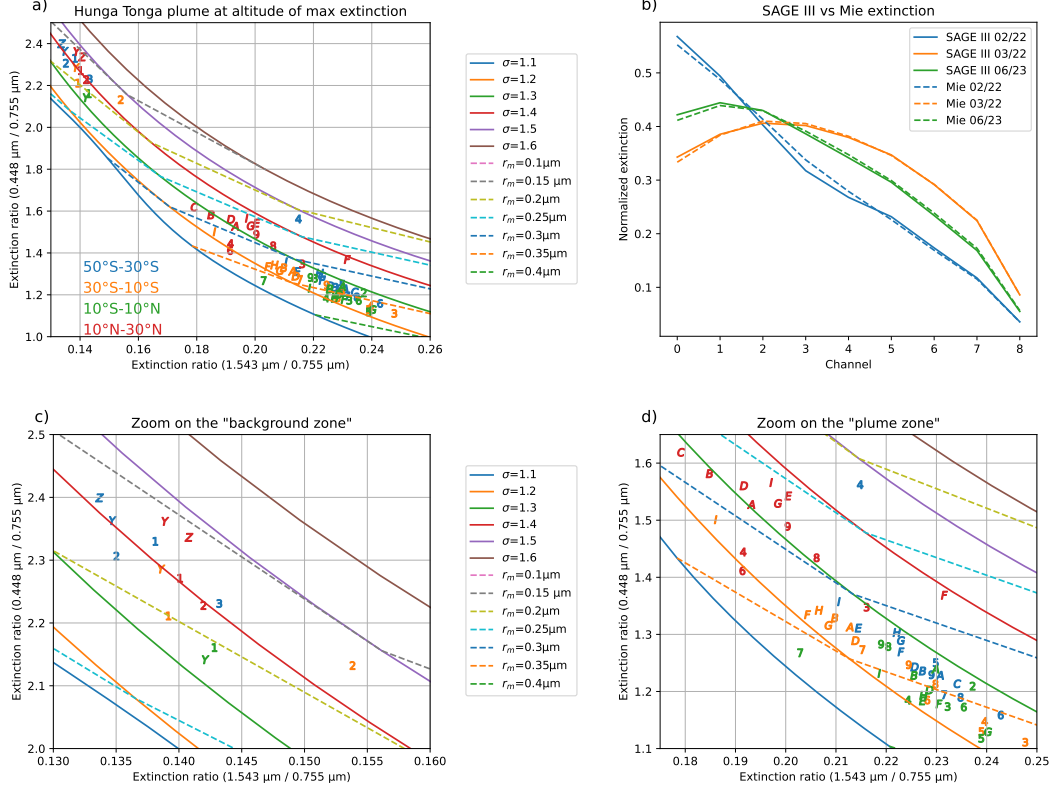


**Figure 1.** (a) The solid curves correspond to Mie calculations of the extinction ratios 448/755 nm and 1,543/755 nm for constant values of the width  $\sigma$ . The dashed curves correspond to constant values of the mean radius  $r_m$ . This panel uses the same axis as Figure 2a of Wrana et al. (2021). The numbers and letters show SAGE III measured ratios for each latitude band (color coded) and month at the central level of maximum 755 nm extinction for each month. The months are coded as Y and Z for November and December 2021, as 1 to 9 between January and September 2022 and alphabetically from A to I between October 2022 and June 2023. For each latitude band, the altitude levels for months before February 2022 (and March for the 40°S band) are chosen to be the same as the central level for the first detection in March 2022 (or April for the 40°S band). (b) Comparison of SAGE III (solid) and modeled (dash) normalized extinctions for all nine aerosol channels of SAGE III. The curves are shown for the latitude band 30°-10°S using the values of  $\sigma$  and  $r_m$  determined from the diagram (a). We show the background case of February 2022 (blue) and the earliest and latest case of the plume in March 2022 (orange) and June 2023 (green). (c, d) are respectively zooms on the "background zone" and the "plume zone" of panel (a).

In the estimation of the two extinction ratios mentioned above, the  $N_0$  parameter cancels out, and we are left with a dependency on  $\sigma$  and  $r_m$  only. Figure 1a shows that the curves for equal  $\sigma$  and  $r_m$  form a skewed grid in the domain of interest allowing the identification of the two parameters. The separation of spectral channels in terms of wavelengths in the two ratios is critical to obtain such results as shown by Wrana et al. (2021). For each data point from SAGE III extinctions the corresponding  $\sigma$  and  $r_m$  values are obtained by interpolating linearly between the discretized curves shown in Figure 1a. Then, the particle effective radius  $r_{\text{eff}}$  can be estimated as  $r_{\text{eff}} = r_m \exp\left(\frac{5}{2} \ln^2 \sigma\right)$ . Finally, we can compute the total number density  $N_0$  from Equation 2 using the extinction at 755 nm. The estimate is retrieved for each profile point with extinction ratios falling between the curves  $\sigma = 1.1$  and  $\sigma = 1.6$  in Figure 1a. This is enough to discard all contributions near or below the tropopause.

The good performance of the method can be appreciated from Figure 1b where modeled Mie extinctions using  $\sigma$  and  $r_m$  drawn from Figure 1a are compared to the SAGE III measured extinctions for three cases, one in the background and two in the plume at 1-year distance. We see that the agreement is excellent over the whole range in spite of the obvious differences between the background and the plume cases. This is consistent with the absence of a coarser mode due to ash in the plume but does not rule out the presence of a finer mode which cannot be distinguished by extinction measurements (von Savigny & Hoffmann, 2020). The fact that estimates of sizes from fall speed (Schoeberl et al., 2022; Legras et al., 2022; Khaykin et al., 2022) using measurements by limb scatter or lidar backscatter and from lidar derived Angström exponent (Baron et al., 2023) are of the order or larger than our own estimate is an indication that such a fine mode is not important here as the lidar measurements in particular would be much more sensitive to it than solar occultation measurements (von Savigny & Hoffmann, 2020).

### 2.3 Estimation of the $\text{H}_2\text{SO}_4$ Total Mass

The  $\text{H}_2\text{SO}_4$  mass is estimated for each vertical layer and latitude band from the estimated values of  $\sigma$  and  $r_m$  in this domain. The volume proportion of  $\text{H}_2\text{SO}_4$  in a droplet is  $\gamma(w_s) = (1 + \frac{\rho_s}{\rho_w}(\frac{1}{w_s} - 1))^{-1}$  where  $\rho_s$  is the density of pure  $\text{H}_2\text{SO}_4$  and  $\rho_w$  is the water density, and the  $\text{H}_2\text{SO}_4$  mass of the droplet is  $m_p(r, w_s) = \frac{4}{3}\pi r^3 \gamma(w_s) \rho_s$ .

Integrating over the lognormal distribution, we find that the  $\text{H}_2\text{SO}_4$  mass contained in a layer centered at latitude  $\phi$  is :

$$m_l = V_l(\phi) \cdot m_p(r_m, w_s) \cdot \alpha(\sigma) \cdot N_0 \quad (3)$$

where  $\alpha(\sigma) = \exp(\frac{9}{2} \ln^2 \sigma)$  is the lognormal volume ratio and  $V_l(\phi) = 4\pi R^2 H \cos(\phi) \sin(\Delta\phi/2)$  is the volume of the layer with  $R = 6,371$  km and  $H = 500$  m.

Summing  $m_l$  over all the layers of the plume, we calculate the total mass for each month and each latitude band for a given  $w_s$ . Unless otherwise specified, we use  $w_s = 0.70$ . The dependency of  $m_l$  upon  $w_s$  is a 2 % increase for an increase of 0.01.

## 3 Results

The first row of Figure 2 shows that the aerosol plume has persisted as a distinguished layer in the stratosphere until June 2023, 17 months after the eruption. Until May 2022 the plume was mainly contained between 30°S and 10°N and then started to spread towards higher latitudes in the southern hemisphere. In spite of the detection of filaments at high latitudes (Mishra et al., 2022; Khaykin et al., 2022), there was little spread beyond the equatorial band in the northern hemisphere. The plume descended constantly until November 2022 but with a latitude dependent speed, in agreement with the Brewer-Dobson circulation, the descent being faster at high latitudes. Since November 2022, the maximum extinction altitude has been stalling at mid-latitudes and slightly rising in the

equatorial band. It is noticeable that for all latitudes north of 30°S the aerosol layer does not disperse in altitude and keeps a fairly constant thickness.

In Figure 1a (see also the zooms in Figures 1c and 1d), the observed extinction ratios at the level of maximum extinction in the plume are distributed over a domain of the diagram that clearly differs from the background points. These latter match the values reported in Wrana et al. (2021) with width  $\sigma$  of 1.4-1.5 and radius  $r_m$  of 0.15-0.2  $\mu\text{m}$ . Instead, all the plume points south of 10°N but a couple of outliers lay between the 1.2 and 1.3  $\sigma$  curves and cluster around  $r_m \approx 0.35 \mu\text{m}$ . This finding of low  $\sigma$  values is important, since usually very different assumptions are made, for example, in satellite limb-scatter retrievals or in size retrievals using a two wavelength-extinction-ratio approach, which can introduce strong retrieval biases. The part of the plume in the 10°-30°N range forms a separate cluster with smaller radius between 0.25 and 0.30  $\mu\text{m}$  and  $\sigma \approx 1.3$ . April 2022 for the 40°S latitude band is a mixed case between background and plume conditions when aerosols begin to reach these latitudes (as seen on Figure 2, first row). Figure S2 shows that retrieval uncertainties do not jeopardize the separation between the background and the plume. It also shows that at all latitudes the mean size decreases with time albeit by a small amount but no trend can be detected for the width. From  $\sigma$  and  $r_m$ , we calculate  $r_{\text{eff}}$  which is near 0.4  $\mu\text{m}$  in the plume while we find 0.2  $\mu\text{m}$  or less for the background in agreement with Khaykin et al. (2022).

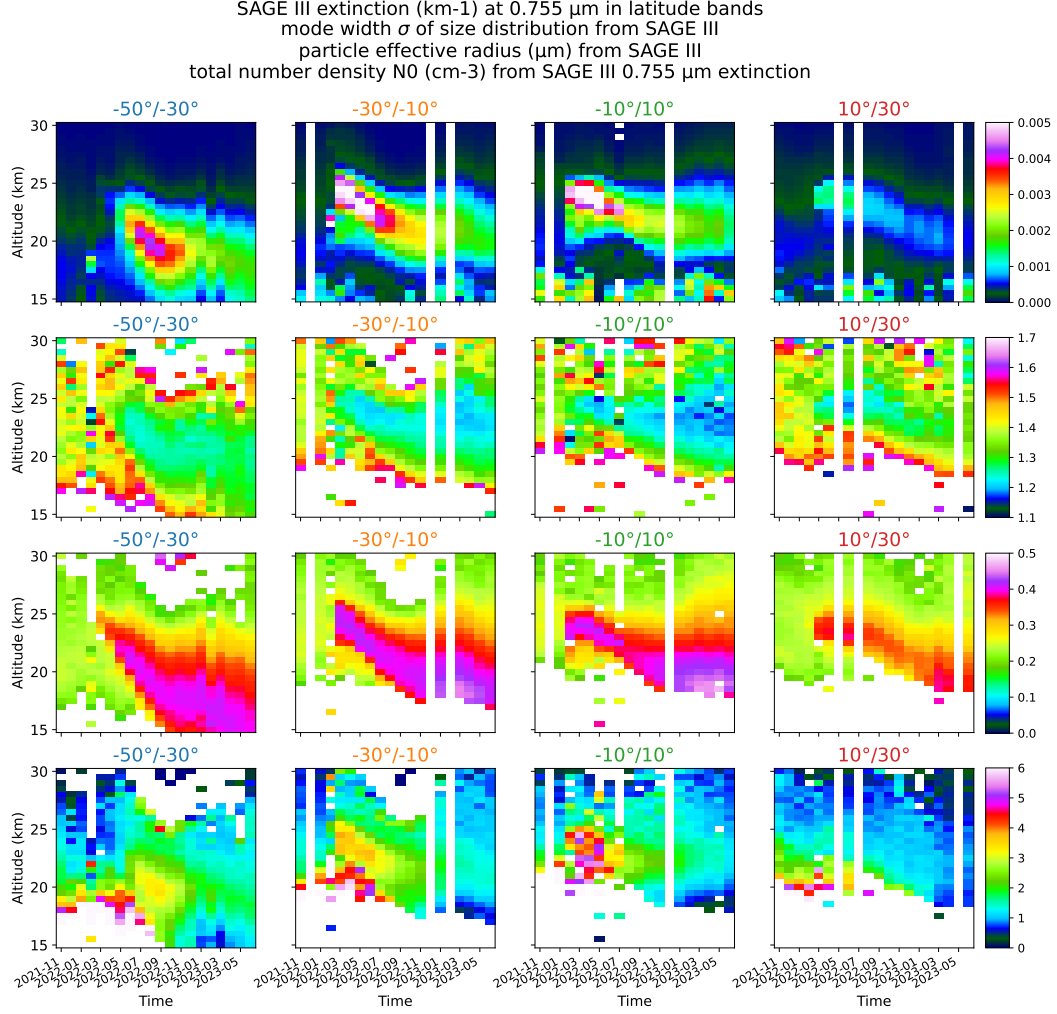
The full temporal evolution of  $\sigma$  and  $r_{\text{eff}}$  is shown in the second and third rows of Figure 2. The homogeneity and the persistence of the properties across the plume and in time are clearly visible. Using the same method, Wrana et al. (2023) found  $\sigma$  values for other stratospheric volcanic plumes produced by the eruptions of Ambae in 2018, Raikoke and Ulawun in 2019, and La Soufrière in 2021, which are all larger, approaching 1.8-2.0 together with smaller sizes (Wrana et al., 2023), reinforcing the exceptional aspect of the HTHH eruption.

Our size estimate is compatible with other estimates of large sizes from radiative remote sensing or in situ measurements of the core part of the plume ( $r_{\text{eff}} > 0.3 \mu\text{m}$  for Baron et al. (2023) and  $r_{\text{eff}} \approx 0.5 \mu\text{m}$  for Kloss et al. (2022) and Boichu et al. (2023)) about 10 days after the eruption while a very few measurements with smaller sizes have also been reported for early dates (Khaykin et al., 2022; Boichu et al., 2023) or peripheral parts of the plume (Kloss et al., 2022). We retain that the stable distribution measured from SAGE III was established just after the fast initial conversion to sulfates.

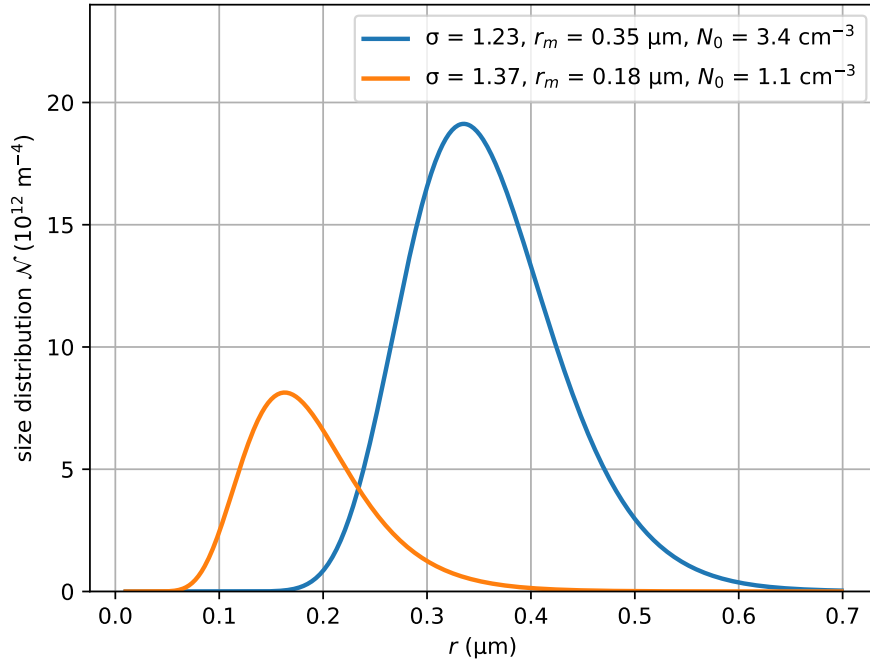
The total number density  $N_0$  is shown in the last row of Figure 2. The largest values of about  $5 \text{ cm}^{-3}$  are found in the early stage of the equatorial band. Values of  $3.5 \text{ cm}^{-3}$  are maintained until September 2022 and are slowly declining afterwards. This density is not very different from that of the background, here around  $2 \text{ cm}^{-3}$  at the altitudes of the plume and  $3 \text{ cm}^{-3}$  for Wrana et al. (2021) at 20 km in June 2017. For comparison, Wrana et al. (2023) found density of 20-30  $\text{cm}^{-3}$  in stratospheric volcanic plumes generated by other recent eruptions with similar sulfur injection but much smaller particles.

Figure 3 shows two retrieved PSD in the same latitude band and altitude range for the background conditions and the plume. We stress that the HTHH eruption actually led to a much wider size distribution than in the background, even though the mode width  $\sigma$  is strongly reduced. This is because  $\sigma$  is the distribution width in logarithmic radius space, not linear radius space.

Figure 4a shows the total amount of  $\text{H}_2\text{SO}_4$  mass in the plume SA and the background mass contribution in the volume of the plume, according to Equation 3 for a value of the mass proportion  $w_s$  of 70%. The total amount between 50°S and 30°N remains remarkably constant from March 2022 to November 2022 in spite of a considerable redistribution in latitude which is shown in Figure 4b. The fast transport to the equato-



**Figure 2.** Zonal altitude-time sections averaged over  $20^\circ$  latitude bands between  $50^\circ\text{S}$  and  $30^\circ\text{N}$  from November 2021 to June 2023. The first row represents the aerosol extinction  $k_{ext}$  ( $\text{km}^{-1}$ ) provided by SAGE III at  $755 \text{ nm}$ . The second row represents the mode width  $\sigma$  of the particle size distribution (PSD) retrieved from SAGE III extinction ratios. The third row represents the particle effective radius  $r_{\text{eff}}$  ( $\mu\text{m}$ ). The fourth row represents the total number density  $N_0$  ( $\text{cm}^{-3}$ ) of the PSD retrieved from SAGE III extinction ratios and  $755 \text{ nm}$  extinction  $k_{ext}$ .



**Figure 3.** Monthly averaged particle size distributions from the retrieved particle size distribution parameters in the  $30^\circ$ - $10^\circ\text{S}$  latitude range. Orange curve corresponds to background conditions at 24.5 km averaged between months of November 2021 and January 2022, blue curve corresponds to plume conditions at altitude of maximum extinction averaged between months of June and August 2022.



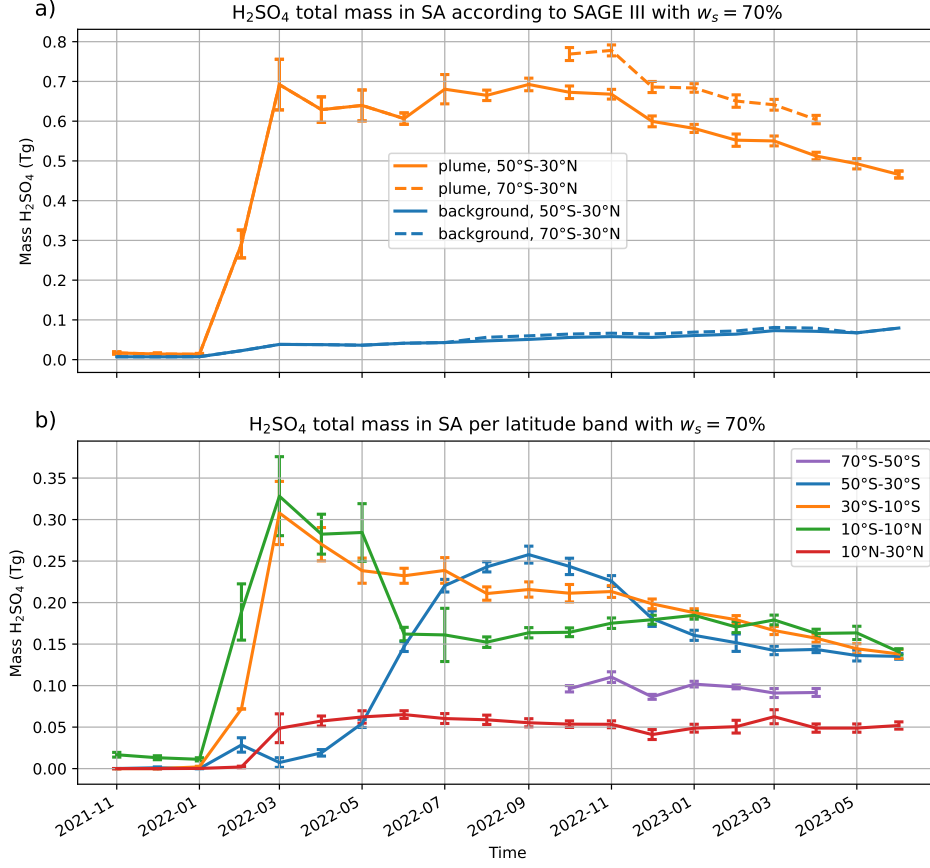


**Figure 4.** (a) Orange curves: evolution of the  $\text{H}_2\text{SO}_4$  total mass contained in the plume sulfates for a  $\text{H}_2\text{SO}_4$  weight percentage  $w_s = 70\%$ , according to SAGE III, eliminating surrounding pixels with radius  $r_m$  less than  $0.2 \mu\text{m}$  considered as background. Blue curves: background contribution within the volume of the plume with  $\sigma = 1.4$ ,  $r_m = 0.15 \mu\text{m}$  and  $N_0 = 1 \text{ cm}^{-3}$ . The latitude range is  $50^\circ\text{S}$ - $30^\circ\text{N}$  for solid curves and  $70^\circ\text{S}$ - $30^\circ\text{N}$  for dashed curves. (b) Evolution of the  $\text{H}_2\text{SO}_4$  total mass per latitude band. The contribution from the  $50^\circ$ - $70^\circ\text{S}$  is zero before May 2022, then is missing until August and contaminated by polar stratospheric clouds until September. It is shown only from October 2022 to April 2023.

rial band during the first month following the eruption mentioned by Schoeberl et al. (2023) generates an equatorial dominance until May 2022 which is followed by a transport to the 40°S band which dominates from August to November 2022. The total mass decline after November 2022 is mainly due to this latitude band, presumably because of the sedimentation towards the lowest stratosphere and return to the troposphere. The equatorial band and the 20°S band essentially exchange aerosol mass while maintaining a constant sum from August 2022 onward. Taking into account the high latitude contribution in the southern hemisphere, which can only be estimated from October 2022 to April 2023, adds 0.1 Tg to the total but does not contribute to the decline. If a distribution of sulfate representing a background component (to be subtracted) is taken into account within the volume of the plume (see Figure 4a), this represents a small correction which increases with the volume of the plume but is always less than 0.1 Tg. Accounting these errors, we estimate the total mass of  $\text{H}_2\text{SO}_4$  between March and November 2022 to be  $0.66 \pm 0.1$  Tg for  $w_s = 70\%$ . It scales proportionally to  $w_s$  if another value is assumed.

Converting the  $\text{H}_2\text{SO}_4$  total mass into a  $\text{SO}_2$  source using the molar mass ratio produces an estimate of 0.44 Tg of  $\text{SO}_2$  for 0.66 Tg of  $\text{H}_2\text{SO}_4$  which is in good agreement with the early estimates (Millán et al., 2022; Carn et al., 2022) produced from satellite observations.

## 4 Conclusions

The HTHH eruption led to a large perturbation in stratospheric aerosols still visible 17 months after the eruption in solar occultation measurements of the satellite instrument SAGE III/ISS. The comparison of these measurements with theoretical Mie calculations supports the hypothesis of the absence of any optical signature of ash. Assuming a monomodal size distribution of liquid spherical SA, we estimate the mode width and the effective radius to the unusual values of  $\sigma \approx 1.25$  and  $r_{\text{eff}} \approx 0.4 \mu\text{m}$  which have persisted at the plume peak height over 17 months with only a small decreasing trend in the size. The additional estimate of the total number density leads to an estimate of the total mass of stratospheric  $\text{H}_2\text{SO}_4$  which is near 0.66 Tg for a mass proportion of 70% and has been found to be very stable over the period March 2022–November 2022 after which it slowly declines. This mass matches very well previous estimates of the stratospheric  $\text{SO}_2$  source of about 0.4–0.5 Tg (Millán et al., 2022; Carn et al., 2022).

The unusual size distribution of aerosols is related to the fast conversion of  $\text{SO}_2$  to sulfates and possible sustained condensation/coagulation under very moist conditions documented by, for example, Legras et al. (2022) and modeled by Zhu et al. (2022). The size distribution is characterized by larger particles than recent stratospheric volcanic eruptions, like Raikoke and others, but smaller than for the Pinatubo (Boichu et al., 2023), with an unusually small mode width. The top of the atmosphere radiative impact has been estimated dominated by the warming of water vapour during the first months after the eruption (Sellitto et al., 2022). Due to the lack of any fast removal of water vapour, this effect is likely to have persisted while the aerosol distribution was stable and to increase while it is decaying.

## Open Research Section

SAGE III/ISS L2 Solar Event Species Profiles V053 data set is available from [https://doi.org/10.5067/ISS/SAGEIII/SOLAR\\_NetCDF4\\_L2-V5.3](https://doi.org/10.5067/ISS/SAGEIII/SOLAR_NetCDF4_L2-V5.3). miepython is a free package available from <https://miepython.readthedocs.io/en/latest/> and <https://doi.org/10.5281/zenodo.8023972>. We used version 2.3.0 in this study. AERIS has provided access to the GEISA database at <https://geisa.aeris-data.fr>.

## Acknowledgments

This study has been supported by the Agence Nationale de la Recherche under Grant 21-CE01-0007-01 (ANR ASTuS) and the Centre National d'Études Spatiales (CNES). Work at the University of Greifswald was funded by the Deutsche Forschungsgemeinschaft (DFG Research Unit VolImpact, Grant 398006378).

## References

- Armante, R., Scott, N., Crevoisier, C., Capelle, V., Crepeau, L., Jacquinet, N., & Chédin, A. (2016, September). Evaluation of spectroscopic databases through radiative transfer simulations compared to observations. Application to the validation of GEISA 2015 with IASI and TCCON. *Journal of Molecular Spectroscopy*, *327*, 180–192. doi: 10.1016/j.jms.2016.04.004
- Baron, A., Chazette, P., Khaykin, S., Payen, G., Marquestaut, N., Bègue, N., & Duflot, V. (2023). Early Evolution of the Stratospheric Aerosol Plume Following the 2022 Hunga Tonga-Hunga Ha’apai Eruption: Lidar Observations From Reunion (21°S, 55°E). *Geophysical Research Letters*, *50*(10), e2022GL101751. doi: /10.1029/2022GL101751
- Biermann, U. M., Luo, B. P., & Peter, T. (2000). Absorption Spectra and Optical Constants of Binary and Ternary Solutions of H<sub>2</sub>SO<sub>4</sub>, HNO<sub>3</sub>, and H<sub>2</sub>O in the Mid Infrared at Atmospheric Temperatures. *The Journal of Physical Chemistry A*, *104*(4), 783–793. doi: 10.1021/jp992349i
- Boichu, M., Grandin, R., Blarel, L., Torres, B., Derimian, Y., Goloub, P., ... Riedi, J. (2023). *Growth and global persistence of stratospheric sulfate aerosols from the 2022 Hunga Tonga-Hunga Ha’apai volcanic eruption* [preprint]. doi: 10.22541/essoar.168565384.43597078/v1
- Carn, S. A., Krotkov, N. A., Fisher, B. L., & Li, C. (2022). Out of the blue: Volcanic SO<sub>2</sub> emissions during the 2021–2022 eruptions of Hunga Tonga—Hunga Ha’apai (Tonga). *Frontiers in Earth Science*, *10*, 976962. doi: 10.3389/feart.2022.976962
- Carr, J. L., Horvath, A., Wu, D. L., & Friberg, M. D. (2022). Stereo Plume Height and Motion Retrievals for the Record-Setting Hunga Tonga-Hunga Ha’apai Eruption of 15 January 2022. *Geophysical Research Letters*, *49*, e2022GL098131. doi: 10.1029/2022GL098131
- Cisewski, M., Zawodny, J., Gasbarre, J., Eckman, R., Topiwala, N., Rodriguez-Alvarez, O., ... Hall, S. (2014). The Stratospheric Aerosol and Gas Experiment (SAGE III) on the International Space Station (ISS) Mission. In R. Meynart, S. P. Neeck, & H. Shimoda (Eds.), *Sensors, systems, and next-generation satellites xviii* (Vol. 9241, p. 924107). SPIE. doi: 10.1117/12.2073131
- de Leeuw, J., Schmidt, A., Witham, C. S., Theys, N., Taylor, I. A., Grainger, R. G., ... Kristiansen, N. I. (2021). The 2019 Raikoke volcanic eruption – Part 1: Dispersion model simulations and satellite retrievals of volcanic sulfur dioxide. *Atmospheric Chemistry and Physics*, *21*(14), 10851–10879. doi: 10.5194/acp-21-10851-2021
- Guo, S., Bluth, G. J. S., Rose, W. I., Watson, I. M., & Prata, A. J. (2004). Re-evaluation of SO<sub>2</sub> release of the 15 June 1991 Pinatubo eruption using ultraviolet and infrared satellite sensors. *Geochemistry, Geophysics, Geosystems*, *5*(4). doi: 10.1029/2003GC000654
- Hersbach, H., Bell, B., Berrisford, P., Hirahara, S., Horányi, A., Muñoz-Sabater, J., ... Thépaut, J. (2020). The ERA5 global reanalysis. *Quarterly Journal of the Royal Meteorological Society*, *146*(730), 1999–2049. doi: 10.1002/qj.3803
- Khaykin, S., Podglajen, A., Ploeger, F., Grooß, J.-U., Tence, F., Bekki, S., ... Ravetta, F. (2022). Global perturbation of stratospheric water and aerosol burden by Hunga eruption. *Communications Earth & Environment*, *3*(1), 316. doi: 10.1038/s43247-022-00652-x

- Kloss, C., Sellitto, P., Renard, J.-B., Baron, A., Bègue, N., Legras, B., ... Jégou, F. (2022). Aerosol Characterization of the Stratospheric Plume From the Volcanic Eruption at Hunga Tonga 15 January 2022. *Geophysical Research Letters*, 49(16), e2022GL099394. doi: 10.1029/2022GL099394
- Lambert, A. (2021). *MLS/Aura Level 2 Water Vapor (H<sub>2</sub>O) Mixing Ratio V005*. NASA Goddard Earth Sciences Data and Information Services Center. (Type: dataset) doi: 10.5067/AURA/MLS/DATA2508
- Legras, B., Duchamp, C., Sellitto, P., Podglajen, A., Carboni, E., Siddans, R., ... Ploeger, F. (2022). The evolution and dynamics of the Hunga Tonga–Hunga Ha’apai sulfate aerosol plume in the stratosphere. *Atmospheric Chemistry and Physics*, 22(22), 14957–14970. doi: 10.5194/acp-22-14957-2022
- Loughman, R., Bhartia, P. K., Chen, Z., Xu, P., Nyaku, E., & Taha, G. (2018). The Ozone Mapping and Profiler Suite (OMPS) Limb Profiler (LP) Version 1 aerosol extinction retrieval algorithm: theoretical basis. *Atmospheric Measurement Techniques*, 11(5), 2633–2651. doi: 10.5194/amt-11-2633-2018
- Millán, L., Santee, M. L., Lambert, A., Livesey, N. J., Werner, F., Schwartz, M. J., ... Froidevaux, L. (2022). The Hunga Tonga–Hunga Ha’apai Hydration of the Stratosphere. *Geophysical Research Letters*, 49(13), e2022GL099381. doi: 10.1029/2022GL099381
- Mishra, M. K., Hoffmann, L., & Thapliyal, P. K. (2022). Investigations on the Global Spread of the Hunga Tonga–Hunga Ha’apai Volcanic Eruption Using Space-Based Observations and Lagrangian Transport Simulations. *Atmosphere*, 13(12), 2055. doi: 10.3390/atmos13122055
- O’Callaghan, J. (2022). Burst of underwater explosions powered Tonga volcano eruption. *Nature*, d41586–022–01544–y. doi: 10.1038/d41586-022-01544-y
- Palmer, K. F., & Williams, D. (1975). Optical constants of sulfuric acid; application to the clouds of Venus? *Applied Optics*, 14(1), 208–219. doi: 10.1364/AO.14.000208
- Poli, P., & Shapiro, N. M. (2022). Rapid Characterization of Large Volcanic Eruptions: Measuring the Impulse of the Hunga Tonga Ha’apai Explosion From Teleseismic Waves. *Geophysical Research Letters*, 49(8), e2022GL098123. doi: 10.1029/2022GL098123
- Schoeberl, M. R., Wang, Y., Ueyama, R., Taha, G., Jensen, E., & Yu, W. (2022). Analysis and Impact of the Hunga Tonga–Hunga Ha’apai Stratospheric Water Vapor Plume. *Geophysical Research Letters*, 49(20), e2022GL100248. doi: doi.org/10.1029/2022GL100248
- Schoeberl, M. R., Wang, Y., Ueyama, R., Taha, G., & Yu, W. (2023). The Cross Equatorial Transport of the Hunga Tonga–Hunga Ha’apai Eruption Plume. *Geophysical Research Letters*, 50(4), e2022GL102443. doi: 10.1029/2022GL102443
- Sellitto, P., Podglajen, A., Belhadji, R., Boichu, M., Carboni, E., Cuesta, J., ... Legras, B. (2022). The unexpected radiative impact of the Hunga Tonga eruption of 15th January 2022. *Communications Earth & Environment*, 3(1), 288. doi: 10.1038/s43247-022-00618-z
- Tabazadeh, A., Toon, O. B., Clegg, S. L., & Hamill, P. (1997). A new parameterization of H<sub>2</sub>SO<sub>4</sub>/H<sub>2</sub>O aerosol composition: Atmospheric implications. *Geophysical Research Letters*, 24(15), 1931–1934. doi: 10.1029/97GL01879
- Taha, G., Loughman, R., Colarco, P. R., Zhu, T., Thomason, L. W., & Jaross, G. (2022). Tracking the 2022 Hunga Tonga–Hunga Ha’apai Aerosol Cloud in the Upper and Middle Stratosphere Using Space-Based Observations. *Geophysical Research Letters*, 49(19), e2022GL100091. doi: 10.1029/2022GL100091
- von Savigny, C., & Hoffmann, C. G. (2020). Issues related to the retrieval of stratospheric-aerosol particle size information based on optical measurements. *Atmospheric Measurement Techniques*, 13(4), 1909–1920. doi: 10.5194/amt-13-1909-2020

- Wiscombe, W. J. (1979). *Mie scattering calculations: Advances in technique and fast, vector-speed computer codes* (Vol. 10). National Technical Information Service, US Department of Commerce.
- Wrana, F., Niemeier, U., Thomason, L. W., Wallis, S., & von Savigny, C. (2023). Stratospheric aerosol size reduction after volcanic eruptions. *preprint, 2023*, 1–30. doi: 10.5194/egusphere-2023-837
- Wrana, F., von Savigny, C., Zalach, J., & Thomason, L. W. (2021). Retrieval of stratospheric aerosol size distribution parameters using satellite solar occultation measurements at three wavelengths. *Atmospheric Measurement Techniques*, 14(3), 2345–2357. doi: 10.5194/amt-14-2345-2021
- Zhang, H., Wang, F., Li, J., Duan, Y., Zhu, C., & He, J. (2022). Potential Impact of Tonga Volcano Eruption on Global Mean Surface Air Temperature. *Journal of Meteorological Research*, 36(1), 1–5. doi: 10.1007/s13351-022-2013-6
- Zhu, Y., Bardeen, C. G., Tilmes, S., Mills, M. J., Wang, X., Harvey, V. L., ... Toon, O. B. (2022). Perturbations in stratospheric aerosol evolution due to the water-rich plume of the 2022 Hunga-Tonga eruption. *Communications Earth & Environment*, 3(1), 248. doi: 10.1038/s43247-022-00580-w

# Supplement to "Observation of the aerosol plume from the 2022 Hunga Tonga – Hunga Ha’apai eruption with SAGE III/ISS"

Clair Duchamp<sup>1</sup>, Felix Wrana<sup>2</sup>, Bernard Legras<sup>1</sup>, Pasquale Sellitto<sup>3,4</sup>, Redha Belhadji<sup>3</sup>, Christian von Savigny<sup>2</sup>

<sup>1</sup>Laboratoire de Météorologie Dynamique (LMD-IPSL), CNRS, Sorbonne Université, ENS-PSL, École Polytechnique, Paris, France

<sup>2</sup>Institute of Physics, University of Greifswald, Greifswald, Germany

<sup>3</sup>Univ. Paris Est Créteil and Université de Paris-Cité, CNRS, Laboratoire Interuniversitaire des Systèmes Atmosphériques (LISA-IPSL), Créteil, France

<sup>4</sup>Istituto Nazionale di Geofisica e Vulcanologia (INGV), Osservatorio Etneo (OE), Catania, Italy

## Contents of this file

1. Table S1 in Section S1
2. Figure S1 in Section S2
3. Text to Figure S1 in Section S2
4. Figure S2 in Section S3

## S1 Number of SAGE III profiles

**Table S1.** Number of vertical profiles of SAGE III per latitude band and month.

	70°S-50°S	50°S-30°S	30°S-10°S	10°S-10°N	10°N-30°N
02/2022	317	4	1	44	85
03/2022	32	186	69	70	43
04/2022	93	309	102	88	113
05/2022	0	217	71	5	0
06/2022	0	287	134	113	110
07/2022	0	218	82	1	0
08/2022	45	340	119	99	118
09/2022	56	120	99	69	60
10/2022	393	91	55	61	92
11/2022	59	145	112	45	77
12/2022	263	49	0	0	63
01/2023	94	127	124	93	100
02/2023	237	24	0	40	53
03/2023	48	160	76	72	42
04/2023	77	328	93	91	112
05/2023	0	190	81	13	0
06/2023	0	313	147	113	132

---

Corresponding author: Clair Duchamp, [clair.duchamp@lmd.ipsl.fr](mailto:clair.duchamp@lmd.ipsl.fr)

## S2 Determination of $w_s$

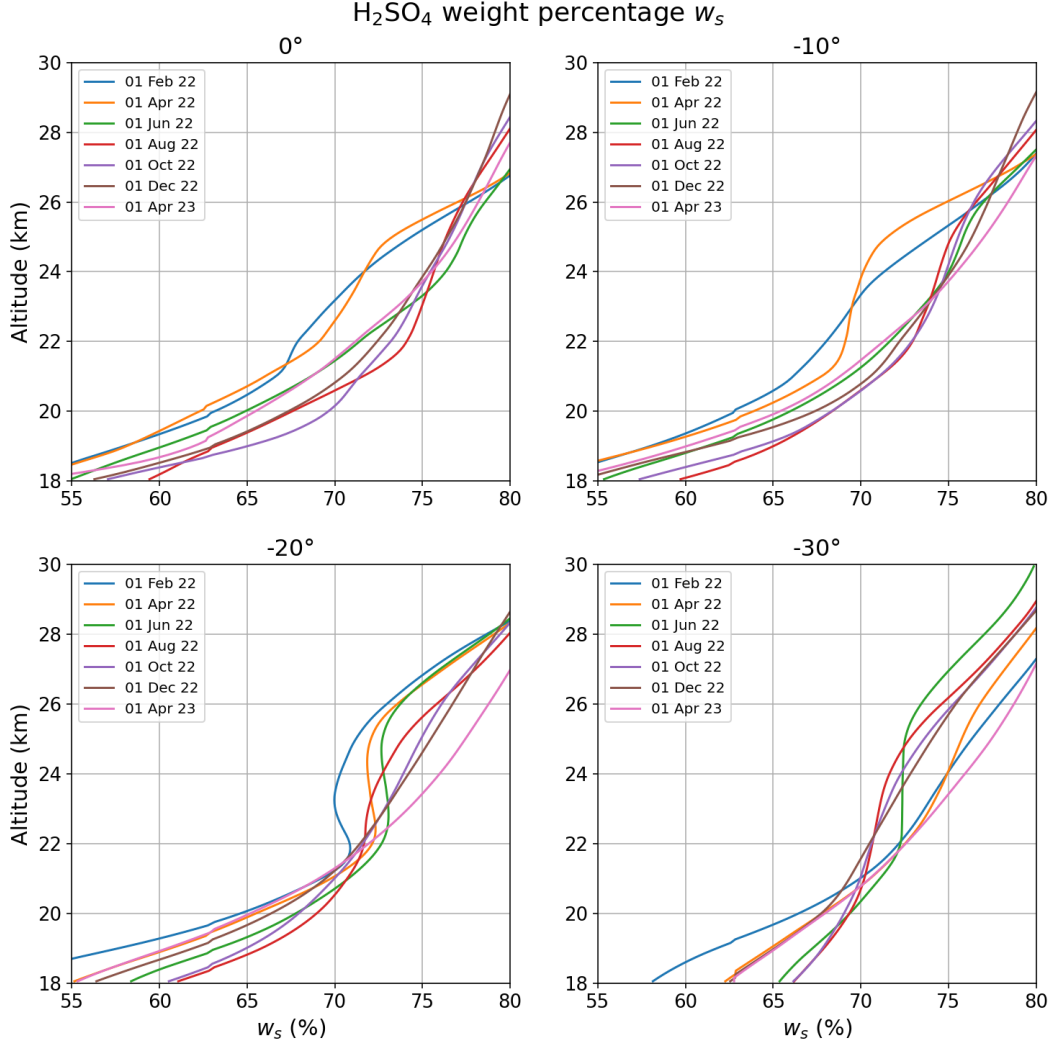


**Figure S1.**  $w_s$  profiles from zonally average profiles of water vapour and temperature at latitudes 0°, 10°S, 20°S and 30°S for a set of dates between February 2022 and April 2023.

We use the water vapour profiles retrieved from the Microwave Limb Sounder (MLS) (Lambert, 2021) in the version 5 and temperature profiles from the ERA5 reanalysis (Hersbach et al., 2020). Zonally average daily profiles of water vapour and temperature are calculated from these datasets. The mass proportion  $w_s$  of sulfuric acid in the sulfate mix is calculated according to Tabazadeh et al. (1997). Fig. S1 shows the  $w_s$  profiles for a set of latitudes and dates in 2022 and 2023. It is noticeable that, for a number of dates, in particular at 20°S and 30°S,  $w_s$  varies little in altitude between 22 and 26 km, that is within the range of altitudes of the plume. It is reasonable to take  $w_s = 70\%$  as a reference mean value during the life-cycle of the plume.

### S3 Evolution of $\sigma$ and $r_m$

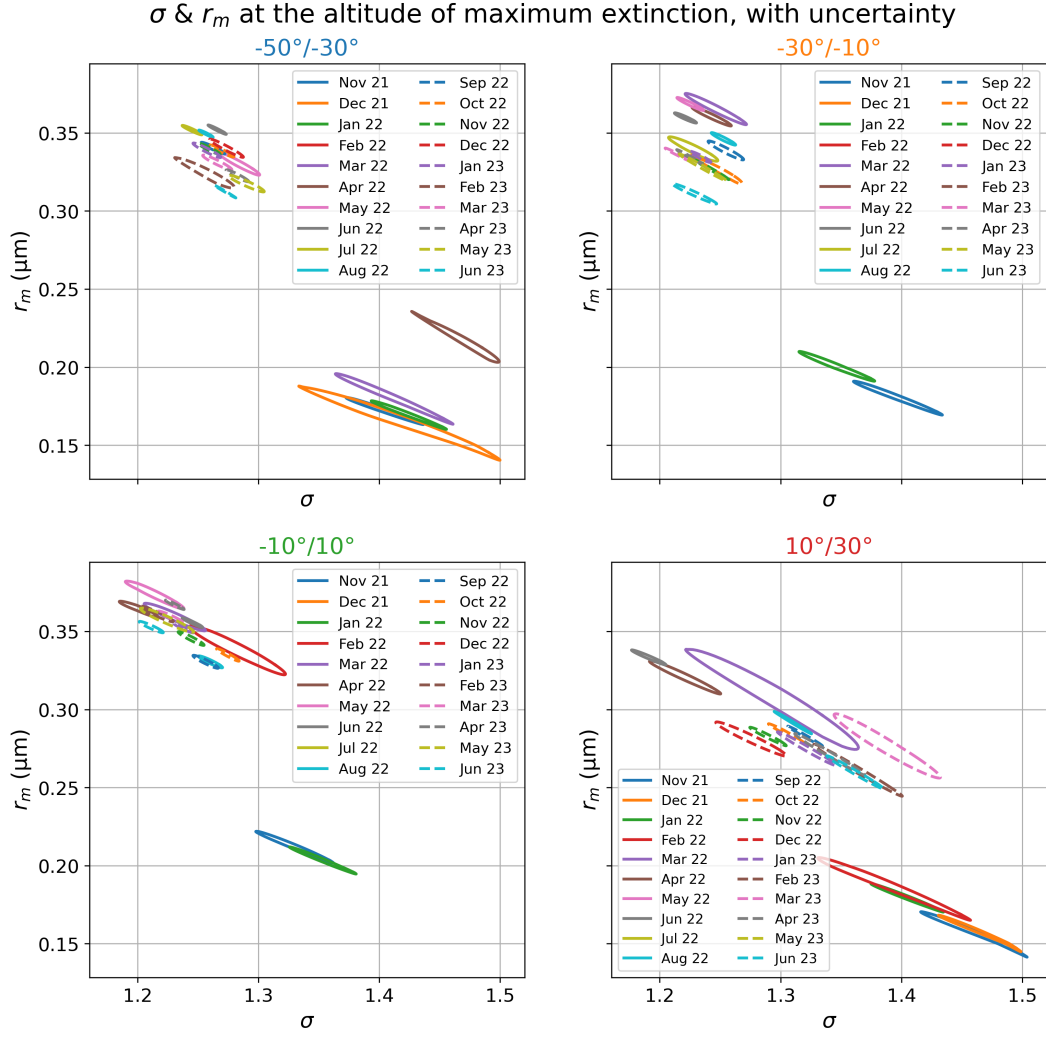


**Figure S2.** Estimates of  $\sigma$  and  $r_m$  at the altitude of the maximum extinction as a function of time. For each month, the uncertainty in  $\sigma$  and  $r_m$  is drawn from the ellipse representing the uncertainty in the two extinction ratios in the plane of Fig. 1a.



## References

- Hersbach, H., Bell, B., Berrisford, P., Hirahara, S., Horányi, A., Muñoz-Sabater, J., ... Thépaut, J. (2020). The ERA5 global reanalysis. *Quarterly Journal of the Royal Meteorological Society*, 146(730), 1999–2049. doi: 10.1002/qj.3803
- Lambert, A. (2021). *MLS/Aura Level 2 Water Vapor (H<sub>2</sub>O) Mixing Ratio V005*. NASA Goddard Earth Sciences Data and Information Services Center. (Type: dataset) doi: 10.5067/AURA/MLS/DATA2508
- Tabazadeh, A., Toon, O. B., Clegg, S. L., & Hamill, P. (1997). A new parameterization of H<sub>2</sub>SO<sub>4</sub>/H<sub>2</sub>O aerosol composition: Atmospheric implications. *Geophysical Research Letters*, 24(15), 1931–1934. doi: 10.1029/97GL01879